An Affordable Millimeter-Wave Beam-Steerable Antenna Using Interleaved Planar Subarrays

Abbas Abbaspour-Tamijani, *Student Member, IEEE,* and Kamal Sarabandi, *Fellow, IEEE*

***Abstract*—Design and fabrication aspects of an affordable planar beam steerable antenna array with a simple architecture are considered in this paper. Grouping the elements of a phased array into a number of partially overlapped subarrays and using a single phase shifter for each subarray, generally results in a considerable reduction in array size and manufacturing costs. However, overlapped subarrays require complicated corporate feed networks and array architectures that cannot be easily implemented using planar technologies. In this paper a novel feed network and array architecture for implementing a planar phased array of microstrip antennas is presented that enables the fabrication of low-sidelobe, compact, beam-steerable millimeter-wave arrays and facilitates integration of the RF front-end electronics with the antenna structure. This design uses a combination of series and parallel feeding schemes to achieve the desired array coefficients. The proposed approach is used to design a three-state switched-beam phased array with a scanning width of $\pm 10^{\circ}$. This phased array which is composed of 80 microstrip elements, achieves a gain of $>$20 dB, a sidelobe level of < -19 dB and a 10-dB bandwidth of $>$6.3% for all states of the beam. The antenna efficiency is measured at 33–36% in X band. It is shown that the proposed feeding scheme is insensitive to the mutual coupling among the elements.**

***Index Terms*—Beam steering, interleaved subarrays, millimeter-wave antennas, phased arrays, subarray overlapping.**

I. Introduction

SINCE the advent of the array theory and development of the early beam-steerable phased arrays in 1960s [1], phase shifters have been widely recognized as the most complex, sensitive, and perhaps expensive parts of the phased array systems. Over the years, array designers have tried to simplify the design process by resorting to powerful full-wave numerical techniques in conjunction with built-in optimization methods [2]–[4]. Also Significant advancement in MMIC and the emerging RF-MEMS technologies has provided the designers with compact and more reliable phase shifters [5], [6]. Yet, with the complexities in the corporate feed and phase control networks, and their interactions with the radiating elements, implementation of the large phase arrays remains a challenging engineering problem. This is particularly true where a large number of phase shifters and an accurate phase control are required.

Manuscript received February 12, 2002; revised May 15, 2002. This work was supported by Mitsubishi Electronics, Osaka, Japan.

The authors are with the Radiation Laboratory, Department of Electrical Engineering and Computer Science, University of Michigan, Ann Arbor, MI 48109-2122 USA (e-mail: abbasa@engin.umich.edu; sarabband@eecs.umich.edu).

Digital Object Identifier 10.1109/TAP.2003.816331

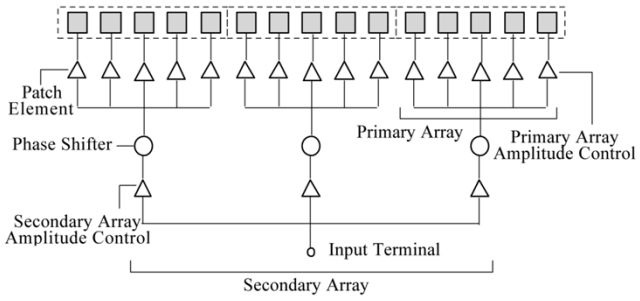

Fig. 1. Grouping of the elements in a phased array.

In military and space applications, tolerances are usually very tight due to the stringent requirements on the antenna sidelobe level and the fact that narrow beams and wide scan angles are often sought for. In recent years on the other hand, phased arrays are being considered for new applications such as commercial millimeter-wave automotive radars and robotic sensors. Typically, in such applications, a very precise pattern control and a wide scan angle are not required. Instead, other commercial engineering measures such as low cost, low complexity, integrability and ease of manufacturing are the driving criteria. For these applications, switched-beam phased arrays with a reduced number of phase shifters may provide a simple and affordable alternative. Although such simplified arrays generally fail to retain a low sidelobe level for the large values of scan angle, they can meet the system requirements for some of these new commercial systems, such as the forward-looking collision avoidance radars, radar sensors monitoring traffic at intersections, and sensors used for navigation.

The idea of reducing the number of phase shifters by dividing a large array into a number of in-phase subarrays and using a single phase shifter for each subarray has been proposed by a number of researchers in the past [7], [8]. This concept has been illustrated in Fig. 1. The underlying concept is to replace the linear-phase profile of the array excitation by its coarse staircase approximation. The array elements are divided into the groups of in-phase elements, or subarrays, and each subarray is fed through a single phase shifter. These subarrays can be viewed as the elements of a second phased array. In this work we assume that all subarrays are identical and refer to each one as a *primary array*. The array of the primary arrays is called the *secondary array*. The corresponding array factors are referred to as primary and secondary array factors, and designated by AF_1 and AF_2, respectively. The combined array factor will be equal to the product of these two array factors.

If the spacing between the subarrays exceeds a maximum value (nearly one wavelength in the broadside design), the secondary array is sparse, and AF_2 will contain grating lobes in the visible region. Even after multiplying by the element factor, presence of these grating lobes can drastically increase the side-lobe level in the overall radiation pattern. This is generally undesirable, as it degrades the beam efficiency. A high side-lobe level also can increase the false alarm rate in the imaging and tracking systems.

As it has been proposed in [9], the sidelobe level may be controlled by a proper choice of the primary array coefficients, so that AF_1 suppresses the unwanted grating lobes of AF_2 in the overall array factor. However, it turns out that for the simple configuration which is obtained by grouping the elements of an equally-spaced array into identical contiguous subarrays,[1] no set of primary array coefficients can be found to provide sufficient attenuation at the grating lobes of AF_2, in the entire scanning range. An additional condition, which is generally referred to as *subarray overlapping*, has to be satisfied in order to resolve this problem [10]. A theoretical derivation of the overlapping condition, along with techniques to realize overlapped subarrays, will be discussed in the next section. For moderate scan angles, subarray overlapping allows for the sidelobe levels of down to -20 dB [11].

Overlapped subarrays may be easily implemented in applications such as radio astronomy and deep space communication, where large arrays of high gain antennas with very large inter-element spacing are used to form extremely narrow beams. However, a planar implementation of the overlapped subarrays proves rather difficult [12], especially when the array is composed of closely spaced low-directivity elements. In such circumstances the mutual coupling between the antenna elements becomes a major obstacle for realizing the desired array coefficients. Another difficulty in the planar implementation of the overlapped subarrays with constraint feed structures is implementing the crossovers in the intersecting subarray feed networks. A commonly used approach is to design the feed network as a combination of hybrid couplers, which allow cross-feeding by successive formation of sums and differences of the input signals [12]. Such feed networks are relatively complicated, need significant real estate, and their accuracy is limited by the performance of the hybrid couplers. In addition, due to the lengthy signal paths, this feeding scheme and its variations are lossy in millimeter-wave frequencies.

As mentioned before, the mutual coupling between the elements of the overlapped subarrays complicates the design task. The difficulty is exacerbated when the array is made to scan. This is due to the fact that changing the relative phase of the array coefficients varies the amount of mutual coupling between the elements. Therefore it is very difficult, if not impossible, to design an array which is impedance matched and properly excited in all states of operation, unless these mutual effects are minimized. Apart from mutual coupling minimization, it is also important to design the feed network so that the subarray excitation coefficients remain insensitive to the mutual coupling. Techniques to address these two tasks, along with an efficient implementation of the feed-line crossovers are the main objectives of this paper. In Section II, we present a short review of the principles of the subarray overlapping technique, and show how this technique may be used to obtain a one-dimensional (1-D) scanning array with a reduced number of phase shifters and a reasonably low sidelobe level. In Section III, the practical aspects of designing a prototype array composed of 80 microstrip antennas are considered. A new feeding technique which mitigates the effects of mutual coupling is introduced in Section IV. Section V presents numerical simulations and experimental results obtained for a scaled prototype in X band.

[1]A contiguous subarray configuration is by definition such an arrangement in which: a) subarrays do not overlap, b) the total length of the array is equal to the sum of the subarray lengths.

II. Overlapping Condition and Interleaved Subarrays

A. Theory

In the basic array theory, a symmetrical broadside linear array factor is obtained by using an in-phase current distribution (pure real array coefficients). This array factor may be scanned by adding a linear-progressive phase factor to the array coefficients along the array axis. Varying this progressive phase results in a scanning beam. Such a scanning scheme requires one phase shifter per array element.

Using the subarraying scheme, the linear progressive phase distribution is replaced by its staircase approximation. The overall array factor is expressed as the product of the two independently synthesized array factors, AF_1 and AF_2

$$AF(\gamma) = AF_1(\gamma) \times AF_2(\gamma) \tag{1}$$

where γ indicates the polar angle with respect to the array axis. The overall radiation pattern is resulted from multiplying this array factor by the element radiation pattern, F_e. When a progressive phase shift is applied to the subarrays, AF_2 starts scanning, while AF_1 remains unchanged. This concept has been demonstrated graphically in Fig. 2.

When the spacing between the subarrays is larger than a wavelength (in the broadside case), AF_2 contains a number of grating lobes in the visible region $(0 \leq \gamma \leq \pi)$. In an ideal design, these grating lobes are expected to be suppressed by the array factor of the subarray, AF_2. However, it can be shown that in a conventional nonoverlapping placement of the primary arrays, once the main beam of AF_2 scans off the boresight, its grating lobes enter to the main lobe of AF_1 where they are not subject to a substantial attenuation.

For simplicity let us assume that both the primary and secondary array factors are uniform arrays with the array factors given by [13]

$$AF_i(\gamma) = \frac{\sin\left(\pi \frac{L_i}{\lambda} \cos\gamma\right)}{N_i \sin\left(\pi \frac{L_i}{N_i \lambda} \cos\gamma\right)}; \quad i = 1, 2 \tag{2}$$

where λ is the operating wavelength, and N_i represents the number of elements in the primary $(i = 1)$ and the secondary $(i = 2)$ arrays. L_i is the length of the ith array and is defined as:

$$L_i = N_i \times D_i \tag{3}$$

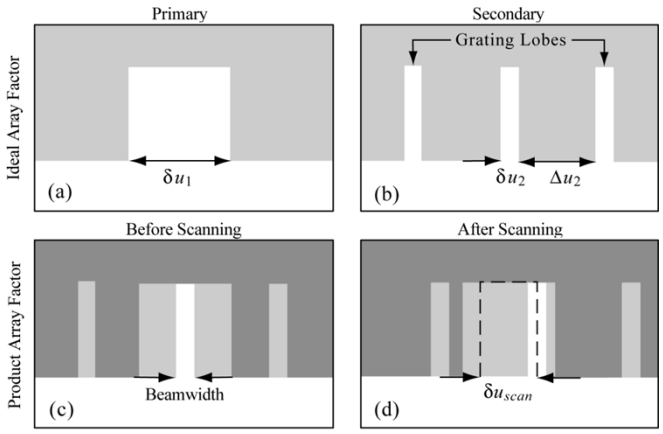

Fig. 2. Array factor multiplication in the grouped arrays. Horizontal axes represents the angle variable u [see (5)]: (a) primary array factor, (b) secondary array factor, (c) overall array factor before scanning, and (d) overall array factor after scanning. All array factors are assumed ideal.

in which D_i represents the inter-element spacing. The actual array factors (1) may be replaced with the idealized gate functions defined by

$$AF_i(\gamma)=\begin{cases}1, & -1\le \frac{L_i}{\lambda}\cos\gamma - qN_i \le 1; q=0,\pm1,\pm2,\dots\\ 0, & \text{elsewhere.}\end{cases} \tag{4}$$

Both (2) and (4) are periodic functions with a limited portion in the visible region, $0 \le \gamma \le \pi$. This periodic behavior is responsible for the existence of the grating lobes. If we define the array angle variable u as

$$u = \frac{2\pi}{\lambda}\cos\gamma \tag{5}$$

the periodicity of the secondary array factor AF_2 as a function of u is given by $\Delta u_2 = 2\pi N_2/L_2$, while the beamwidth of the primary array factor AF_1 is corresponding to $\delta u_1 = 4\pi/L_1$. Let us define the scan-width δu_{scan}, as the separation between the beam centers at the two ends of the scanning range. If we assume that a grating lobe of AF_2 receives enough attenuation so long as at least half of its beamwidth falls outside the main beam of AF_1, referring to Fig. 2(d), this condition can be expressed by

$$\Delta u_2 \ge \frac{1}{2}(\delta u_1 + \delta u_{\text{scan}}). \tag{6}$$

δu_{scan} cannot be greater than δu_1, on the other hand, and may be written as:

$$\delta u_{\text{scan}} = \alpha \delta u_1; \quad 0 \le \alpha < 1. \tag{7}$$

Using (7), (6) is simplified to the following form:

$$\Delta u_2 \ge (1+\alpha)\frac{\delta u_1}{2} \tag{8}$$

which in terms of the array parameter may be written as

$$L_1 \ge (1+\alpha)\frac{L_2}{N_2} = (1+\alpha)D_2. \tag{9}$$

Equation (9) represents the condition on the subarray length and spacing to avoid grating lobes in the overall array factor.

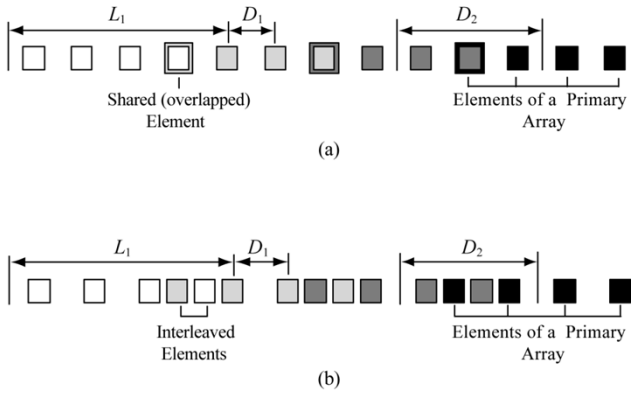

Fig. 3. Two different realizations of subarray overlapping: (a) partially overlapped subarrays and (b) interleaved subarrays.

Considering that D_2 is in fact the distance which is allocated to each subarray in the secondary array, it is useful to define an *overlapping factor*

$$OF = \frac{L_1}{D_2} - 1 \tag{10}$$

which basically represents the fraction of the length of a subarray which overlaps with each of its neighboring subarrays. For the nonoverlapping subarrays $OF \le 0$ (the equality referring to the contiguous subarrays), while for the overlapped subarrays OF is a positive number.

In terms of the overlapping factor, (9) may be rewritten as:

$$OF_{\min} = \alpha = \frac{\delta u_{\text{scan}}}{\delta u_1}. \tag{11}$$

This states that for nonzero scan-width $(\alpha > 0)$, the subarrays must be arranged in an overlapping fashion to avoid grating lobes. The minimum required amount of the overlapping is equal to α.

Although this proof is based on the idealized array factors given by (4), the result is generally true for the actual array factors, once the beam-widths are replaced with half-power beam-widths. However, the overlapping condition may be less stringent in the actual cases $(OF < \alpha)$, as will be seen in the design example presented in the second part of this section.

B. Array Design

There are at least two ways to realize overlapped subarrays. One way is to share one or more of the end elements of the adjacent subarrays, as shown in Fig. 3(a). In this arrangement, each shared elements can be considered as two superimposed elements belonging to two different subarrays, and its excitation coefficient is obtained by adding the respective partial excitation coefficients. This results in an equally spaced array constellation, which is commonly known as *partially overlapped subarrays*.

The second approach is to interleave some of the end elements of the neighboring subarrays [Fig. 3(b)]. Each element belongs to only one subarray in this case, and has a simple excitation coefficient. This constellation may be referred to as *interleaved subarrays*. Even if the elements are equally-spaced in the constituent subarrays, the interleaved subarrays result in a

TABLE I
PARAMETERS OF THE PRIMARY AND SECONDARY ARRAYS

	Primary Array	Secondary Array
Array Length	2.73λ	6.83λ
Inter-Element Spacing	0.68λ	1.71λ
HPBW	22 degs.	8.5 degs.
Sidelobe Level	-20 dB	-19 dB
Array Coefficients	1,1.74,1.74,1	1, 1.66, 1.66, 1

nonuniformly spaced constellation. In this work, however, for the reasons that will become clear, we choose the interleaved subarrays to realize overlapping.

Overlapped subarrays may be designed for a given beamwidth, sidelobe level, and scanning range. The lengths of the primary and secondary arrays (L_1 and L_2) are calculated from the required values of scanning range and beamwidth, respectively. The primary array is designed to provide the required beamwidth and sidelobe level with a minimal number of elements, N_1. The number of elements in the secondary array, N_2, is then set to the minimum for which the grating lobes of AF_2 receive enough suppression from AF_1, under the maximal scanning condition (always $> L_2/L_1$ due to the overlapping). N_2 determines the required number of phase shifters. As the sidelobe level is a primary concern, Dolph–Chebyshev array coefficients [13] are used for both the primary and secondary arrays.

The aforementioned procedure has been used for designing a phased array with a sidelobe level of < -20 dB, a half-power beamwidth (*HPBW*) of 7 °, and a scanning range of ± 10.5 ° (corresponding to a scan-width of ± 7 °). This array is considered for a radar system mounted on a tower for monitoring the railroad crossing intersections. The number of elements in the primary and secondary arrays were found as $N_1 = N_2 = 4$ in this case, resulting in a 16 element array constellation. The values of L_1, L_2, as well as the excitation coefficients for the primary and the secondary arrays are given in Table I. The overlapping factor in this case is 0.6, which is slightly lower than the theoretical minimal value of 0.64, given by (11). The primary array factor is designed for a -20 dB sidelobe level. Assuming a cosine type element factor that provides an extra attenuation of approximately -1 dB at the first sidelobe of AF_2, we design the secondary array factor for a sidelobe level of -19 dB, which is slightly higher than the required. This allows for more flexibility in the design. The corresponding array factors are shown in Fig. 4. Using a cosine type element factor, the overall radiation pattern can be calculated for the boresight and squint beam positions, as presented in Fig. 5.

III. A PLANAR IMPLEMENTATION OF THE INTERLEAVED SUBARRAYS

The array coefficients calculated in the previous section may be used to design a two dimensional array of 16×5 elements with the capability of scanning in the horizontal plane. This array which is shown in Fig. 6, is composed of 16 identical rows, each including five series-fed rectangular microstrip patch antennas. With the Dolph-Chebyshev array coefficients of

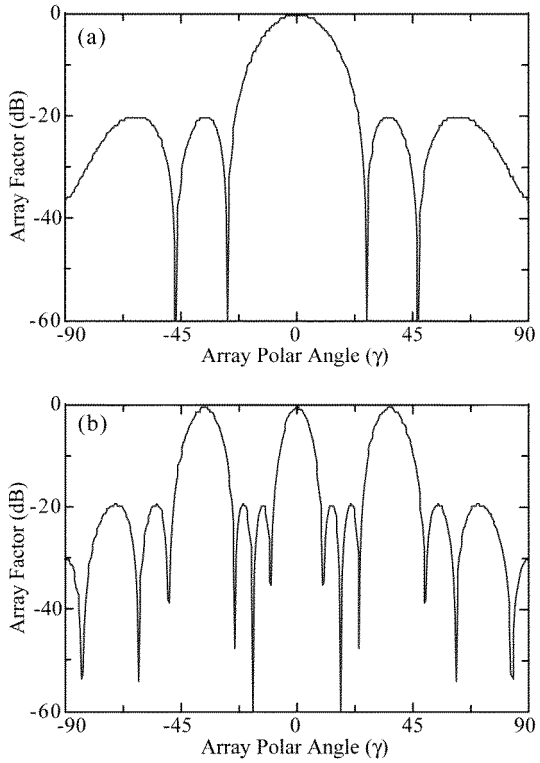

Fig. 4. Synthesized array factors versus the array polar angle γ: (a) primary and (b) secondary.

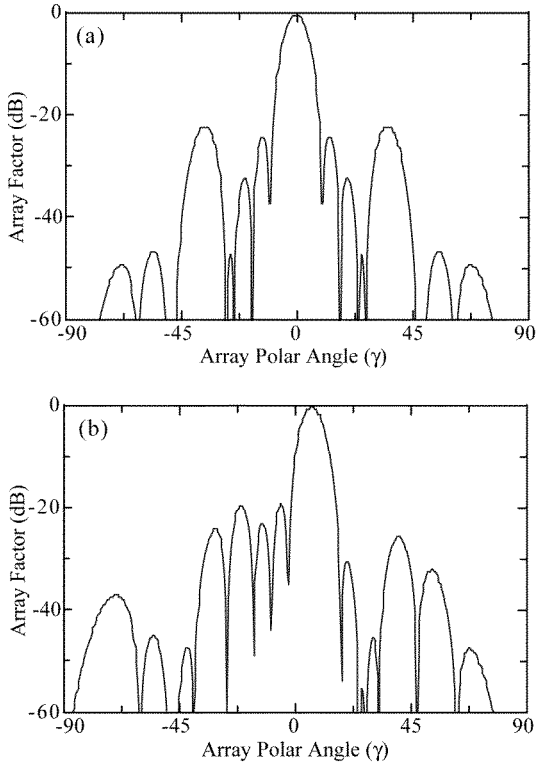

Fig. 5. Radiation pattern of the combined array versus the array polar angle γ: (a) without scanning and (b) with $+7$ ° scanning.

1:1.61:1.93:1.61:1, each vertical row has a narrow-beam pattern with a side lobe level of -20 dB in the vertical plane,

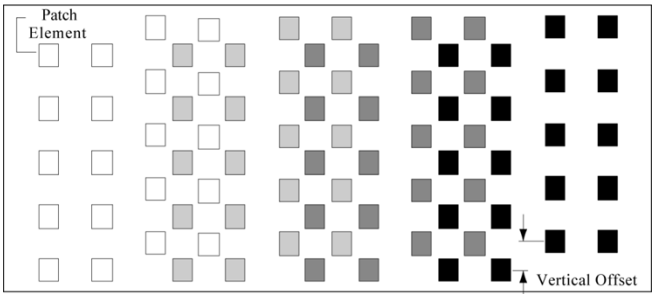

Fig. 6. Simplified layout of the 80 element array; different subarrays are shown in different gray levels.

and a broad-beam cosine type pattern in the horizontal plane. These rows act as the elements of the subarrays, with the excitation coefficients given in Table I. The subarrays are, as a result, 2-D arrays of 4×5 elements, as shown in Fig. 6.

In each row, the array coefficients are implemented through a series of resonant microstrip line sections (see Section IV), which connect the patch elements in the antenna layer. The horizontal array coefficients in each subarray are set to the designed values, using a corporate network of such resonant sections. The corporate feed network lies on a second microstrip layer (feed layer), which is isolated from the antenna layer by a common ground plane. Coupling between the corporate feed and microstrip antennas is achieved through subresonant slots in the ground plane, which are located under the central element of each row. Layouts of the antenna and feed layers are shown in Fig. 7 for an individual subarray. The resonant sections used in this design are simply two-port microwave networks that provide a fixed voltage ratio between the input and output, independent of the loading conditions. Principle of operation and the design procedure for these resonant sections will be described in Section IV.

Each subarray is connected to the secondary array feed network at the input terminal of the corporate feed. Assuming that the subarrays are properly matched at these terminals, a conventional 1-to-4 tree power divider along with phase shifters at its output terminals may be used to realize the desired excitation coefficients for the secondary array (as given in Table I). The power divider and phase shifters are also fabricated on the feed layer. Phase shifters may be realized as the integrated parts of the feed network, or they can be fabricated separately and assembled on the feed network using wire-bonding, or flip-chip techniques.

Layouts of the antenna and feed layers for the full array are shown in Fig. 8. Subarray overlapping is achieved by interleaving the end rows of the neighboring subarrays in the overlapping region. As it has been shown in Fig. 8(a), the interleaved rows are positioned with a vertical offset. Such a vertical displacement does not affect the radiation pattern in the horizontal plane, and since the offset length is small as compared to the length of the rows, its effect on the vertical plane pattern is negligible. The advantage of the offset arrangement of the adjacent rows, on the other hand, is two-fold: 1) it allows the interleaved subarrays to be fed through nonintersecting feed networks, and 2) it reduces the mutual coupling between the closely spaced rows of the interleaved subarrays. Fig. 7(b) shows a subarray

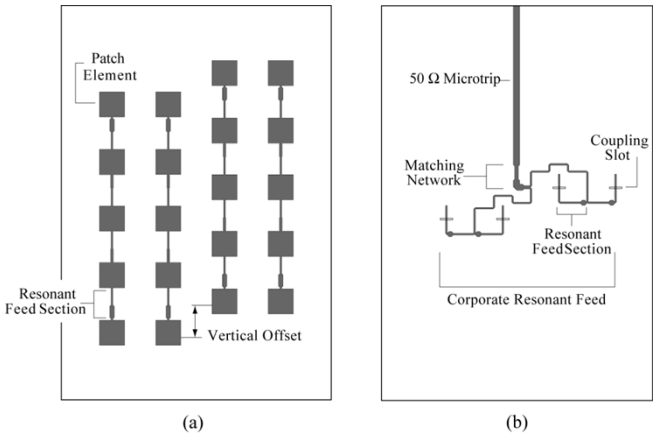

Fig. 7. Subarray layout: (a) antenna layer and (b) feed layer.

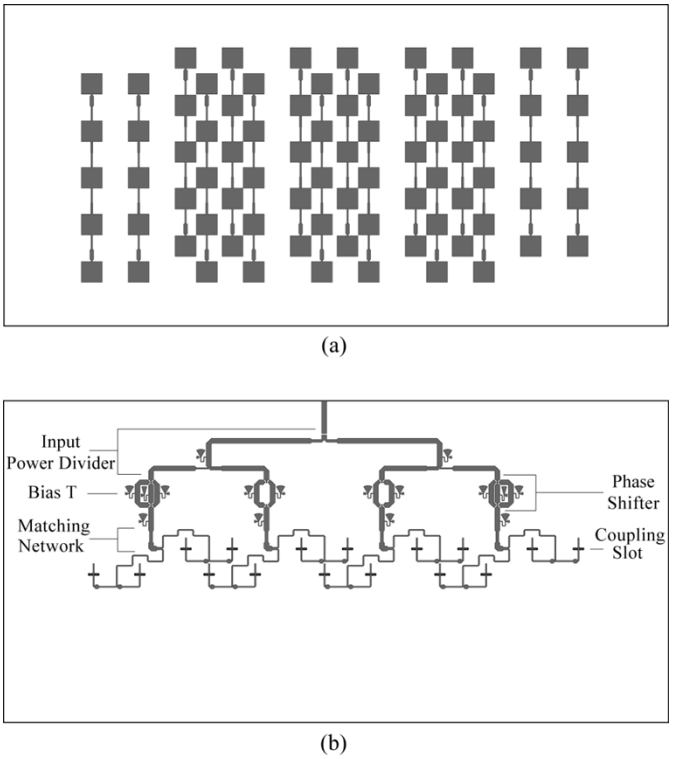

Fig. 8. Layout of the two-layer phased array: (a) antenna layer and (b) feed layer.

corporate feed which has been modified to conform with the offset geometry of the subarray. As shown in Fig. 8(b), such corporate feeds may be used to feed the overlapped subarrays in a nonintersecting fashion.

The effect of vertical offsetting in reducing the mutual coupling between closely spaced elements can be studied using a simple numerical experiment. Fig. 9 shows the simulated value of $|S_{21}|$ between the input terminals of two adjacent rectangular microstrip antennas, as a function of the vertical offset h. The patch antennas are identical to the elements of the array (optimized for operation at 60 GHz), and are positioned with a horizontal center-to-center distance of $d_{\min} = D_1/2$ which is equal to the shortest horizontal separation occurring between the interleaved elements of two neighboring subarrays. It is observed

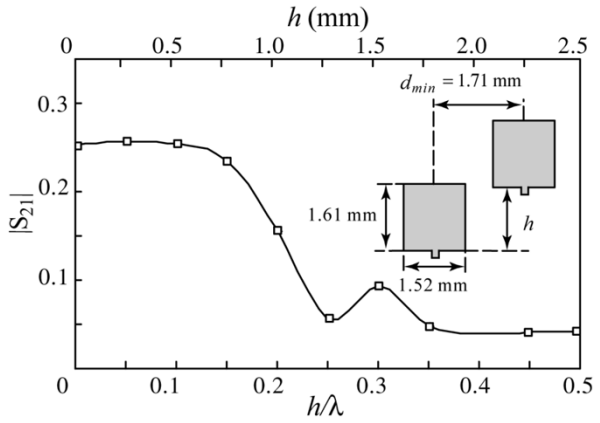

Fig. 9. Mutual coupling between two adjacent patch antennas versus vertical offset.

that the value of $|S_{21}|$, which indicates the mutual coupling, is reduced with increasing the vertical offset, and reaches a minimum for $h = \lambda/4$.

As mentioned earlier, since in a scanning array the amount of mutual loadings are not constant and depend on the state of the beam, in principle it is impossible to account for the mutual coupling in the design of the feed network, and therefore it is important to minimize such effects as much as possible. On this context, the importance of the offset placement of the adjacent elements becomes evident. To further minimize the effect of mutual coupling on the excitation coefficients in a subarray, we introduce the concept of resonant feed network in the next section.

IV. A Novel Array Feeding Approach for Mitigation of Mutual Coupling Effects

To enforce a nodal voltage distribution which is independent of loading, a class of standing-wave feed sections can be designed and placed between the elements of the microstrip array. Assuming that the form of the current distribution over each patch is fixed and the proximity of the other elements only changes the amplitude of this distribution, the input currents $\{I_j\}$ and the edge voltages $\{V_j\}$ of the array elements are related through an admittance matrix $[Y_{j,i}]$. The total input current to the jth patch is given by

$$I_j = Y_{j,j}V_j + \sum_{i\neq j} Y_{j,i}V_i = \left(Y_j^{\rm rad} + \sum_{i\neq j} Y_{j,i}\frac{V_i}{V_j}\right)\times V_j \quad (12)$$

where $Y_j^{\rm rad} = Y_{j,j}$ represents the edge radiative admittance of the element, and $Y_{j,i}$ is the mutual admittance between jth and ith elements. For the given edge voltage ratios V_i/V_j, the coupled network may be replaced by an array of uncoupled admittance loads Y_j^a at the element terminals (usually referred to as the *active admittance* [13]), given by (8)

$$Y_j^a = \frac{I_j}{V_j} = Y_j^{\rm rad} + \sum_{i\neq j} Y_{j,i}\frac{V_i}{V_j} = Y_j^{\rm rad} + Y_j^{\rm ext} \quad (13)$$

where $Y_j^{\rm ext}$ represents the effect of mutual coupling from the other elements in the array.

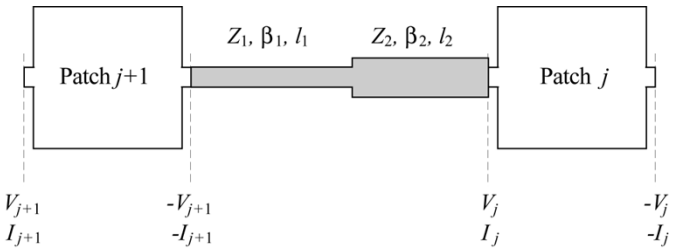

Fig. 10. Two patch elements connected using a two-part transmission line feed section.

Assuming that the feed network establishes the desired edge voltage ratios between the patch elements, the active admittances Y_j^a generally can be calculated from (13) and used for designing the feed network. In our case, however, the voltage distribution over each subarray can also be affected by the coupling from the elements of the neighboring subarrays, which varies with the change of their relative phase of excitation. To eliminate the dependence of the voltage distribution on this variable mutual coupling, the subarray feed network must be designed so that (the ratio of) its terminal voltages are independent of the loading. In the rest of this section, we will describe a procedure for designing such a feed network.

Assume that the edges of two neighboring patch antennas in the array are connected through a two-segment transmission line with electrical lengths $\beta_1 l_1$ and $\beta_2 l_2$ and characteristic impedances Z_1 and Z_2, as shown in Fig. 10. Neglecting the losses in the transmission lines, the $ABCD$ matrix of the two-port transmission line is obtained by multiplying the $ABCD$ matrices of the individual sections

$$\begin{bmatrix} a & b \\ c & d \end{bmatrix} = \begin{bmatrix} \cos\beta_1 l_1 & jZ_1\sin\beta_1 l_1 \\ \frac{j}{Z_1}\sin\beta_1 l_1 & \cos\beta_1 l_1 \end{bmatrix} \times \begin{bmatrix} \cos\beta_2 l_2 & jZ_2\sin\beta_2 l_2 \\ \frac{j}{Z_2}\sin\beta_2 l_2 & \cos\beta_2 l_2 \end{bmatrix}. \quad (14)$$

As for a resonant patch, the voltages between the two opposite edges are related by a factor of -1, the left edge voltage V_{j+1} is related to the left edge voltage and current of the jth patch, V_j and I_j, as

$$\begin{aligned} -V_{j+1} &= aV_j + bI_j \\ &= (\cos\beta_1 l_1\cos\beta_2 l_2 - \frac{z_1}{z_2}\sin\beta_1 l_1\sin\beta_2 l_2 V_j) \\ &\quad + j(Z_2\cos\beta_1 l_1\sin\beta_2 l_2 + Z_1\sin\beta_1 l_1\cos\beta_2 l_2)I_j. \end{aligned} \quad (15)$$

To establish a terminal voltage ratio $V_{j+1}/V_j = K$ which is independent of the terminal currents, (15) requires that $a = -K$ and $b = 0$. Another constraint that is the spacing between the two antenna elements, on the other hand, fixes the total length $l_1 + l_2$ to a given value, l. These conditions may be combined to result in the following set of equations:

$$\begin{aligned} l_1 + l_2 &= l && \text{(a)} \\ \cos\beta_1 l_1 &= -K\cos\beta_2 l_2 && \text{(b)} \\ \frac{Z_1}{Z_2} &= \frac{-\tan\beta_2 l_2}{\tan\beta_1 l_1} && \text{(c)}. \end{aligned} \quad (16)$$

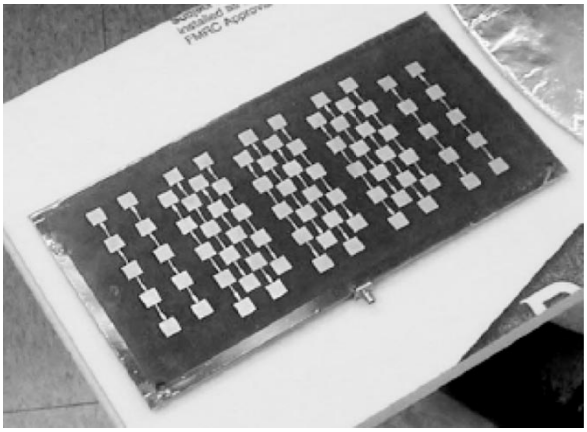

Fig. 11. *X* band prototype of the 80-element array.

Noting that on a given substrate β_1, β_2, Z_1, and Z_2 are functions of the line widths W_1 and W_2, one can solve (16) for l_1, l_2, W_1 and W_2 to achieve the desired voltage ratio K. As the number of unknowns is larger than the number of equations, an extra constraint may be applied, for example by setting the smaller of W_1 and W_2 to the minimum realizable width (here 100 μm). Not for all values of K and l, however, do these equations have a solution which results in a realizable positive admittance ratio. Yet, for typical values of K between 1/3 and 3, and $\beta_1 l_1 + \beta_2 l_2$ between $\pi/2$ and $3\pi/2$, one can normally find a solution with feasible values for Z_1 and Z_2.

It can be shown that the two-segment transmission line obtained in this way has a singular impedance matrix. Hence, we refer to such a structure as a *resonant section*. The relative terminal voltages of all patch elements in a subarray may be fixed by successively locking the terminal voltages of the adjacent elements using such resonant sections. The combination of these resonant sections is called the *resonant feed network*, and has the property that its terminal voltage distribution is independent of the loading. The procedure for designing a resonant feed section has been described in Appendix A, for an example design case.

Although the resonant feed network enforces the desired voltage distribution, it does not provide a straight forward relation between the reactive parts of the input admittance and the terminal loadings. Therefore, it is not possible to design a resonant feed network which simultaneously provides the desired voltage distribution and the input matching. A practical approach is to design the feed network for the voltage distribution, and then calculate or simulate the input impedance of the entire structure. Once the input impedance is known, one can easily use a simple matching network to match the synthesized array. In our case, we use matching networks at the input of each subarray. Aside from the mismatch losses, the impedance matching of the subarrays is essential for proper operation of the phase shifters and the input power divider. A simple matching network can be obtained by cascading two or three transmission line sections. As patch antennas are inherently narrow-band elements, the bandwidth of the matching and resonant feed networks are not of particular importance in the design procedure.

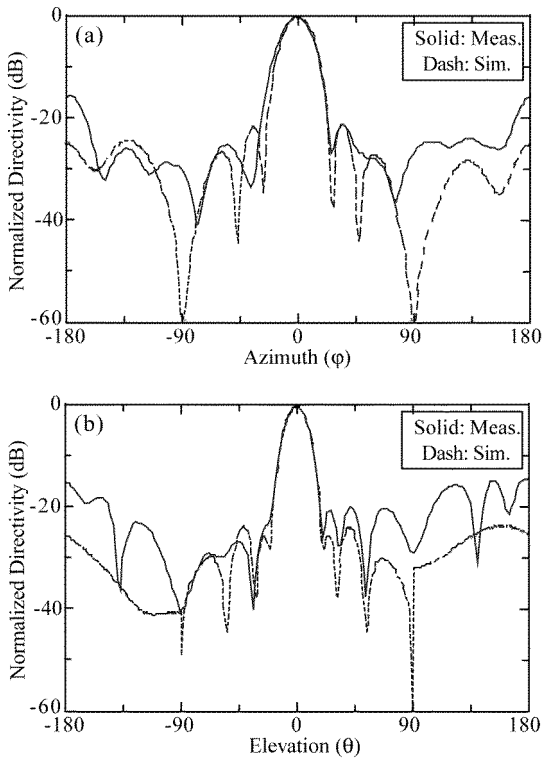

Fig. 12. Measured and simulated radiation patterns for a subarray: (a) horizontal plane and (b) vertical plane.

V. Experimental Results

The $5 \times 4 \times 4$-element array described in Section III is considered for a millimeter-wave traffic control radar operating at 60 GHz. This simple radar system is intended for monitoring a railroad crossing to inform an approaching high speed train of the vehicles and objects that might be on the track. A scaled prototype of this array was fabricated and measured in X band. A photograph of the fabricated prototype is shown in Fig. 11. This array is fabricated on a 0.79 mm-thick Teflon substrate, with a relative permittivity of $\epsilon_r = 2.2$. As the original design was for the same substrate with 0.13 mm thickness, the layout is scaled by a factor of 6.2 to maintain the design properties. The nominal frequency of operation, therefore, is scaled down to 9.68 GHz.

First, a single subarray is fabricated and measured. Fig. 12 shows the measured and simulated radiation patterns in the vertical and horizontal planes. Simulations are performed by the commercial moment-method simulators IE3D [3] and Momentum [2]. In both principal planes, a good agreement between the measurement and simulation is observed. Moreover, if the element factor is extracted (approximately $\cos\varphi$ in the horizontal plane and unity in the vertical plane), these patterns reduce to nearly equi-sidelobe Chebyshev array factors, for which the array coefficients were designed. This indicates that the resonant feed network has successfully set the excitation coefficients to the targeted values. The measured sidelobe level is less than -20 dB in both planes. A return loss of better than 10 dB was measured over a 4% bandwidth for this subarray. These results and some other subarray parameters are summarized in Table II.

TABLE II
MEASURED DATA FOR THE PRIMARY ARRAY

Iteration #	0	1	2	3
Z_1 (Ω)	100	100	100	100
Z_2 (Ω)	50.0	56.6	57.2	57.2
l_1 (mm)	-	1.275	1.264	1.264
l_2 (mm)	-	0.725	0.736	0.736
W_1 (mm)	0.100	0.100	0.100	0.100
W_2 (mm)	0.375	0.308	0.302	0.302
$\epsilon_{r-eff(1)}$	1.724	1.724	1.724	1.724
$\epsilon_{r-eff(2)}$	1.883	1.856	1.854	1.854
α_1 (/m)	2.15	2.15	2.15	2.15
α_2 (/m)	1.85	1.88	1.88	1.88

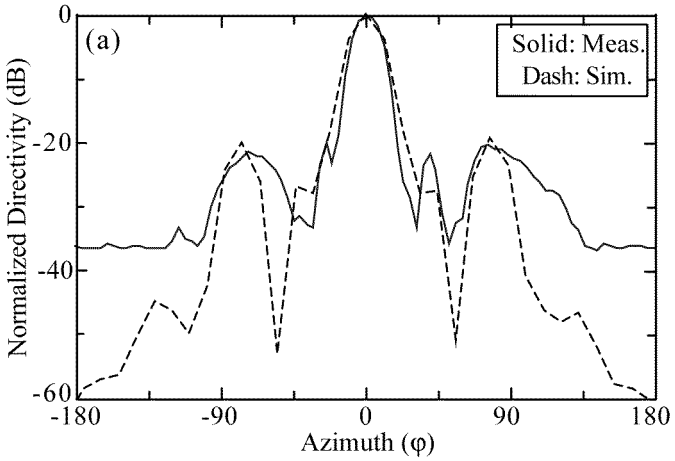

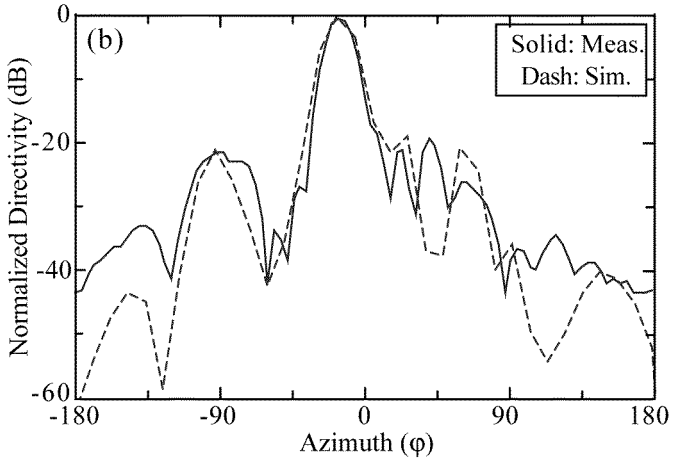

Fig. 13. Measured and simulated radiation patterns of the full array in the horizontal plane; top: boresight beam position, bottom: squint beam position.

TABLE III
MEASURED DATA FOR THE PRIMARY ARRAY

Resonance Frequency	9.68 GHz
-10 dB Bandwidth	4%
HPBW (H†)	22 degs.
HPBW (V‡)	16 degs.
Sidelobe Level (H†)	< -22 dB
Sidelobe Level (V‡)	< -20 dB
Directivity	20.6 dB
Cross-Polarization	< -22 dB

†In horizontal plane, ‡In vertical plane.

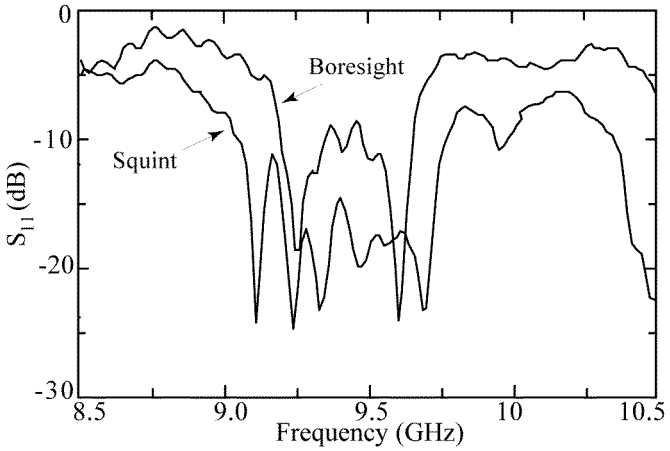

Fig. 14. Measured S_{11} versus frequency in the boresight and squint beam positions.

To form the 80-element array, four subarrays are combined through a corporate feed network. The corporate feed is a two-stage input-matched power divider that is designed to provide the required excitation coefficients for the secondary array, as given in the last column of Table I. Resistors are not used in the design of this power divider, expecting a balanced operation. Two different prototypes are fabricated for the boresight and squint-beam arrays. The phase shifters are replaced by fixed delay lines in these prototypes. Fig. 13 shows the measured and simulated radiation patterns of the 80-element phased array for boresight and squint-beam operation. Only the horizontal plane patterns are shown, as the pattern in the vertical plane is identical to that of the subarrays. Sidelobe levels of -20 dB and -19 dB are measured for the boresight and squint cases, respectively. With a measured beamwidth of 8 ° and 16 ° in the horizontal and vertical planes, the estimated directivity of the array is 25 dB. The measured gain with the beam at the boresight is 20.6 dB, which corresponds to an efficiency of 36%. The losses can be attributed to Ohmic and surface wave losses in the patch elements as well as the feed network. Similarly, in the squint beam position the calculated directivity and measured gain are 24.8 dB and 20 dB, respectively, which results in an efficiency of 33% in this case.

The measured return loss of the full array is presented in Fig. 14. The 10-dB bandwidth of the array is observed to be 6.3% and 8.5% for the beam at boresight and squint positions, respectively. In both cases a broader bandwidth is observed as compared to the subarray case, which is believed to be due to the presence of the power divider which along with the subarray matching networks forms a higher order input matching. Although these bandwidths are not symmetrically spanned around the design frequency of 9.68 GHz, a pseudo-resonance is observed near this frequency. The bandwidth enhancement in the squint beam position may be attributed to the out-of-phase interference of the partial reflected signals from different subarrays, which reduces the total reflected power. The measured performance data of the 80-element prototypes are listed in Table III.

VI. Conclusion

In this paper, we demonstrated that the fabrication complexity of the beam-steerable phased array systems can be drastically reduced by using subarraying techniques. The fundamental concepts and practical issues were explored, and a design procedure was developed. It was shown that low sidelobe levels may be achieved for a relatively narrow scan angle. The effectiveness of this method becomes evident when a scanning array with high angular resolution and a large number of beam state is required.

A planar implementation of partially overlapped subarrays, suitable for millimeter-wave applications was demonstrated. Using a multitude of innovative approaches, a simple two-layer realization is obtained, which eliminates many problems in both design and fabrication stages. Issues involved in the design of the feed network, as well as the mutual coupling concerns in the layout design were addressed. The concept of resonant feeding was developed and used as a basis for a robust control of the phased array excitation coefficients in a heavy mutual coupling environment. In the applications where a narrow scanning range is required, these techniques may be combined to provide a cost-effective solution. The proposed planar design is conducive for integration of the phased array with the rest of the RF front-end.

Appendix A

Design of Resonant Feed Sections

To show the design procedure, we use (16) to design a resonant section that provides an edge voltage ratio of $K = 1.6$ between the two neighboring patches. We assume that the total length of this section is fixed at 2 mm. At 60 GHz, and on a 125 μm thick teflon substrate ($\epsilon_r = 2.2$), a 100 Ω microstrip line has a width of $W_1 = 100\ \mu$m and $\epsilon_{r-\text{eff}(1)} = 1.72$, and a 50 Ω line has a width of $W_2 = 375\ \mu$m and $\epsilon_{r-\text{eff}(2)} = 1.88$. For the total length of $l = 2$ mm and starting from the values of β_1 and β_2 corresponding to the effective dielectric constants of the 100 Ω and 50 Ω lines, respectively, we may solve (16) numerically to obtain the values of Z_2/Z_1, l_1, and l_2. Fixing Z_1 at 100 Ω, we may use a synthesis program such as LineCalc [2] to determine the new values of W_2 and $\epsilon_{r-\text{eff}(2)}$. This steps are repeated until the results converge. Result of such an iterative procedure are presented in Table IV. α_1 and α_2 in this table show the simulated attenuation constants of the line sections at 60 GHz. They may be used to predict the actual voltage ratio in presence of the transmission line losses, which have been neglected in our derivations. Replacing β_1 with the complex propagation constant $\beta_1 - j\alpha_1$ and β_2 with $\beta_1 - j\alpha_1$ in (15), and using the values in the last column of Table IV, we obtain

$$V_{j+1} = (1.600 + j0.002)V_j + (0.297 + j0.000)I_j. \quad (17)$$

This shows that for the terminal loading impedances of $\geq 10\ \Omega$, the terminal voltage ratio of this section varies within less than 2% Table IV of the desired value of 1.6.

TABLE IV
Iterative Design of an Example Resonant Section

	Boresight	Squint
Center Frequency	9.45 GHz	9.40 GHz
-10 dB Bandwidth	6.3%	8.5%
HPBW (H†)	8.0 degs.	8.5 degs
Sidelobe Level (H†)	< -20 dB	< -19 dB
Directivity	25.0 dB	24.8 dB
Gain	20.6 dB	20.0 dB
Efficiency	36 dB	33 dB

†In horizontal plane.

References

[1] N. Fourikis, *Phased Array-Based Systems and Applications*. New York: Wiley, 1997.

[2] Advanced Design System, Agilent Technologies 2002, Santa Clara, CA.

[3] IE3D 7.0, Zeland Software Inc., TX, USA.

[4] Picasso, Emag Technologies Incorporated, Ann Arbor, MI.

[5] J. S. Hayden, A. Malczewski, J. Kleber, C. L. Goldsmith, and G. M. Rebeiz, "2 and 4-bit DC to 18 GHz microstrip MEMS distributed phase shifters," in *Proc. IEEE MTT-S Intl. Microwave Symp. Dig.*, 2001, pp. 219–222.

[6] H. Nayashi, T. Nakagawa, and K. Araki, "A miniaturized mimic analog phase shifter using two quarter-wave-length transmission lines," *IEEE Trans. Microwave Theory Tech.*, vol. 50, pp. 150–154, Jan. 2002.

[7] J. T. Nemit, "Network Approach for Reducing the Number of Phase Shifters in a Limited Scan Phased Array," U.S. Patent 380 362 5, 1974.

[8] R. J. Mailloux and P. R. Franchi, "Phased Array Antenna With Array Elements Coupled to Form a Multiplicity of Overlapped Subarrays," U.S. patent 3 938 160, 1976.

[9] R. J. Mailloux, L. Zahn, A. Martinez, and G. Forbes, "Grating lobe control in limited scan arrays," *IEEE Trans. Antennas Propagat.*, vol. 27, pp. 79–85, Jan. 1979.

[10] R. L. Fante, "Sysytem study of overlapped subarrayed scanning antennas," *IEEE Trans. Antennas Propagat.*, vol. 28, pp. 668–679, Sept. 1980.

[11] R. J. Mailloux, "A low sidelobe partially overlapped constrained feed network for time delayed subarrays," *IEEE Trans. Antennas Propagat.*, vol. 49, pp. 280–291, Feb. 2001.

[12] S. P. Skobelev, "Methods of controlling optimum phased-array antennas for limited field of view," *IEEE Antennas Propagat. Mag.*, vol. 40, pp. 39–40, Apr. 1998.

[13] R. S. Elliott, *Antenna Theory and Design*. Englewood Cliffs, NJ: Prentice-Hall, 1981.

Abbas Abbaspour-Tamijani (S'00) received the B.S. and M.S. degrees in electrical engineering from The University of Tehran, Tehran, Iran, in 1994 and 1997, respectively. He is currently pursuing the Ph.D. in electrical engineering, with emphasis on applied electromagnetics and RF circuits, at The University of Michigan at Ann Arbor.

From 1997 to 1999, he worked as an RF and Antenna Engineer in the telecommunication industry. In the academic year 1999–2000, he was a visitor at the Antenna Laboratory, University of California at Los Angeles (UCLA), where he was involved with the design of feed systems for space-borne reflector antennas. In Fall 2000, he joined The Radiation Laboratory of The university of Michigan at Ann Arbor. His research area includes RF microelectromechanical systems and components, phased arrays and focal plane scanning systems, and integrated front-ends.

Kamal Sarabandi (S'87–M'90–SM'92–F'00) received the B.S. degree in electrical engineering from Sharif University of Technology, Tehran, Iran, in 1980, the M.S. degree in electrical engineering, the M.S. degree in mathematics, and the Ph.D. degree in electrical engineering from The University of Michigan, Ann Arbor, in 1980, 1986, and 1989, respectively.

Currently, he is the Director of the Radiation Laboratory and a Professor in the Department of Electrical Engineering and Computer Science at the University of Michigan. His research areas of interest include microwave and millimeter-wave radar remote sensing, electromagnetic wave propagation, and antenna miniaturization. He has 20 years of experience with wave propagation in random media, communication channel modeling, microwave sensors, and radar systems and is leading a large research group including two research scientists, ten Ph.D. and two M.S. students. Over the past ten years, he has graduated 14 Ph.D. students. He has served as the Principal Investigator on many projects sponsored by NASA, JPL, ARO, ONR, ARL, NSF, DARPA and numerous industries. He has published many book chapters and more than 95 papers in refereed journals on electromagnetic scattering, random media modeling, wave propagation, antennas, microwave measurement techniques, radar calibration, inverse scattering problems, and microwave sensors. He has also had more than 200 papers and invited presentations in many national and international conferences and symposia on similar subjects.

Dr. Sarabandi was the recipient of the prestigious Henry Russel Award from the Regent of The University of Michigan (the highest honor the University of Michigan bestows on a faculty member at the assistant or associate level). In 1999 he received a GAAC Distinguished Lecturer Award from the German Federal Ministry for Education, Science, and Technology given to about ten individuals worldwide in all areas of engineering, science, medicine, and law. He was also a recipient of a 1996 Teaching Excellence Award from the EECS Department of The University of Michigan. In the past several years, joint papers presented by his students at a number of symposia (IEEE AP'95,'97,'00,'01, IEEE IGARSS'99, IEEE MTTS'01) have received student prize paper awards. He is serving as the Associate Editor of the IEEE TRANSACTIONS ON ANTENNAS AND PROPAGATION (AP) and the IEEE SENSORS JOURNAL. He is a Vice President of the IEEE Geoscience and Remote Sensing Society (GRSS), Chairman of the Awards Committee of the IEEE GRSS, and a Member of IEEE Technical Activities Board Awards Committee. He is a Member of Commission F of URSI and of The Electromagnetic Academy. Professor Sarabandi is listed in *American Men & Women of Science*, *Who's Who in America*, and *Who's Who in Electromagnetics*.